

Nanosilver suppresses growth and induces oxidative damage to DNA in *Caenorhabditis elegans*

Piper Reid Hunt^{a*}, Bryce J. Marquis^{b†}, Katherine M. Tyner^c, Sean Conklin^d, Nicholas Olejnik^a, Bryant C. Nelson^b and Robert L. Sprando^a

ABSTRACT: Studies on the effects of nanomaterial exposure in mammals are limited, and new methods for rapid risk assessment of nanomaterials are urgently required. The utility of *Caenorhabditis elegans* cultured in axenic liquid media was evaluated as an alternative *in vivo* model for the purpose of screening nanomaterials for toxic effects. Spherical silver nanoparticles of 10 nm diameter (10nmAg) were used as a test material, and ionic silver from silver acetate as a positive control. Silver uptake and localization, larval growth, morphology and DNA damage were utilized as endpoints for toxicity evaluation. Confocal reflection analysis indicated that 10nmAg localized to the lumen and tissues of the digestive tract of *C. elegans*. 10nmAg at 10 $\mu\text{g ml}^{-1}$ reduced the growth of *C. elegans* larvae, and induced oxidative damage to DNA as measured by 8-OH guanine levels. Consistent with previously published studies using mammalian models, ionic silver suppressed growth in *C. elegans* larvae to a greater extent than 10nmAg. Our data suggest that medium-throughput growth screening and DNA damage analysis along with morphology assessments in *C. elegans* could together provide powerful tools for rapid toxicity screening of nanomaterials. Published 2013. This article is a US Government work and is in the public domain in the USA.

Additional Supporting Information may be found in the online version of this article.

Keywords: nanosilver; silver ions; growth suppression; DNA damage; endotoxin; toxicity screen

Introduction

Nanomaterials can be produced in a variety of sizes and shapes and with a multitude of coatings, giving them unique properties which permit their use in a variety of applications in many commercial markets. As a consequence, the probability for human exposure to nanomaterials from a variety of sources is growing rapidly. Nanoparticle size and coating have been associated with specific toxic effects in a number of *in vivo* and *in vitro* systems (Choi & Hu, 2008; Ellegaard-Jensen *et al.*, 2012; Kvittek *et al.*, 2008; Lok *et al.*, 2007; Meyer *et al.*, 2010; Zhang *et al.*, 2003), and it has been reported that the shape of nanomaterials can greatly influence their biological activity (Pal *et al.*, 2007). It is therefore imperative that rapid and efficient means of nanomaterial toxicity screening be developed so that each individual type of nanoparticle can be assessed for safety. While some information on human toxicity can be gathered after the fact from accidental toxic exposures (Fung & Bowen, 1996), most toxicity data are gathered either from *in vitro* testing using model systems such as cell culture, or *in vivo* using model organisms such as rats and mice. Questions about the lack of correlation between *in vitro* and *in vivo* studies (Parry *et al.*, 2010; Sayes *et al.*, 2007), and the high cost and long duration of rodent studies (Lee *et al.*, 2012), make small invertebrate models such as *Caenorhabditis elegans* attractive *in vivo* alternatives for risk assessment. Additionally, Congress has mandated that alternative test methods which replace mammals with 'phylogenetically lower animal species' be developed and validated (Congress, 2000). To address this mandate, several government agencies including the National Institutes of Health

and the U.S. Food and Drug Administration are collaborating to assess the predictive capacity of economically efficient model systems for toxicity testing (HHS/NIH, HIEHS/NTP, NHGRI/NCGC, EPA/ORFDA, 2010).

The advantages of using the nematode *C. elegans* as an alternative toxicological testing model include its small size, short generation time and ease of culture, which allow the rapid generation of data on a large number of test animals at low cost. Additionally, the *C. elegans* transparent external cuticle allows observation of internal organs and individual cells in live animals

*Correspondence to: Piper Reid Hunt, United States Food and Drug Administration, Center for Food Safety and Applied Nutrition, Office of Applied Research and Safety Assessment, Division of Toxicology, Laurel, MD 20708, USA. E-mail: Piper.Hunt@fda.hhs.gov

^aUnited States Food and Drug Administration, Center for Food Safety and Applied Nutrition, Office of Applied Research and Safety Assessment, Division of Toxicology, Laurel, MD 20708, USA

^bNational Institute of Standards and Technology, Material Measurement Laboratory, Gaithersburg, MD 20899, USA

^cUnited States Food and Drug Administration, Center for Drug Evaluation & Research, Silver Spring, MD 20993, USA

^dUnited States Food and Drug Administration, Center for Food Safety and Applied Nutrition, Office of Regulatory Sciences, College Park, MD 20740, USA

[†]Present address: University of Central Arkansas, Department of Chemistry, Conway, AR 72035, USA

for efficient morphology analyses. *C. elegans* lack a respiratory system and their external cuticle is quite tough, limiting their usefulness in predicting toxicity from inhalation or dermal routes of exposure. However, their very simplicity and the fact that they continuously intake environmental liquid and suspended particles via a pharyngeal pumping mechanism (Avery & You, 2012), make them a potential model for oral exposure.

A simple model organism will only prove useful for risk analyzes if test results can predict outcomes in more complex organisms. Given that *C. elegans* homologs have been identified for 60 to 80 percent of human genes and many key regulatory proteins and signal transduction pathways are conserved (Kaletta & Hengartner, 2006; Kawasaki *et al.*, 1999), and that significant correlations have been found between toxicity ranking in *C. elegans* and rat (Boyd *et al.*, 2010a; Cole *et al.*, 2004; Ferguson *et al.*, 2010; Hunt *et al.*, 2012; Williams & Dusenbery, 1988), this small nematode is likely to prove an excellent model in which to screen nanomaterials for toxicity.

Nanosilver has bacteriocidal and bacteriostatic properties (Morones *et al.*, 2005; Sondi & Salopek-Sondi, 2004), and inhibits the formation of biofilms (Percival *et al.*, 2007) which can act as barriers to antimicrobial agents and host immune responses. Because of these antibiotic activities, nanosilver is the largest and fastest growing class of nanomaterials used in consumer products (Fabrega *et al.*, 2011; Wijnhoven *et al.*, 2009). However, there is increasing evidence that the use of nanosilver is not without risk. Toxic effects associated with *in vitro* nanosilver exposure include the induction of DNA damage in mouse embryonic stem cells and fibroblasts (Ahamed *et al.*, 2008) and reduced mitochondrial function and membrane integrity in rat liver cells (Hussain *et al.*, 2005). *In vivo* nanosilver effects have been observed in fish, with increased mortality and delayed hatching in nanosilver exposed *Danio rerio* (zebrafish) (Asharani *et al.*, 2008), and cellular and DNA damage as well as expression of stress response genes in *Oryzias latipes* (medaka) (Chae *et al.*, 2009).

It is important to distinguish between nanosilver and ionic silver. Nanoparticles are defined as objects that are between 1 and 100 nm in at least one dimension. Nanosilver is a cluster of silver atoms that can be manufactured in various sizes and shapes. Ionic silver consists of silver atoms missing a single electron, giving them a crystal ionic radius of approximately 0.1 nm. While utilized in medical applications for centuries (Alexander, 2009), ionic silver is known to be toxic to humans (Berger *et al.*, 1976; Drake & Hazelwood; 2005; Fung & Bowen, 1996). Ionic silver causes hypoactivity in mice (Rungby & Danscher, 1984) and reduced growth and eventually death in rats (Matuk *et al.*, 1981). Both ionic silver and nanosilver bioaccumulate, and are excreted in urine and feces (Dziendzikowska *et al.*, 2012; Fung & Bowen, 1996). The antibiotic activity of nanosilver has been shown to be as effective, or more effective, than ionic silver in several previous studies (Choi & Hu, 2009; Fabrega *et al.*, 2009; Sotiriou & Pratsinis, 2010), making nanosilver an attractive alternative antibiotic.

In order to facilitate the risk assessment process, it is imperative that potential hazards associated with nanosilver exposure be investigated further (Bonner, 2010; Foldbjerg *et al.*, 2011). DNA damage in cultured mammalian cells is induced by silver nanoparticles in the 6 to 25 nm range (Ahamed *et al.*, 2008; Asharani *et al.*, 2009a), and for mouse lymphoma cells treated with $5 \mu\text{g ml}^{-1}$ of 5-nm silver, this damage was shown to be oxidative in nature (Mei *et al.*, 2012). The number of published reports on the *in vivo* toxic effects from the oral

ingestion of nanosilver in mammals is limited (Dziendzikowska *et al.*, 2012; Loeschner *et al.*, 2011). In one rat study, ingestion of 60-nm silver at 30, 300 or 1000 mg kg⁻¹ body weight per day did not affect body weight, however, there was evidence of slight liver damage at the intermediate and high doses (Kim *et al.*, 2008). In another rat study that only looked at distribution after 9 mg kg⁻¹ body weight per day of either 14-nm silver or ionic silver, organ distribution was similar for the two types of silver, however, absolute silver concentrations in tissues were lower in the nanosilver treated group than in the ionic silver treated group, whereas fecal silver concentrations were higher in the nanosilver-treated group, indicating reduced bioabsorption of nanosilver relative to ionic silver (Loeschner *et al.*, 2011). Additionally, a recent rat study found that while 9 mg kg⁻¹ body weight per day of 14-nm silver had no effect on weight gain over a 28-day period, equimolar ionic silver from silver acetate did significantly reduce weight gain (Hadrup *et al.*, 2012). Together these data indicate that lower doses of nanosilver may be safe for mammalian consumption, that ionic silver is more toxic than nanosilver and that oxidative DNA damage induced by smaller species of nanosilver may still be a concern. We hypothesized that these findings of reduced toxicity of nanosilver relative to ionic silver and nanosilver induced oxidative damage to DNA and would be replicated in *C. elegans*.

The standard laboratory method of culturing *C. elegans* utilizes agar plates seeded with a lawn of *Escherichia coli* as a food source (Brenner, 1974). With this standard method, cultured worms are transferred individually to treatment plates using a microscope and a very small probe, and later scored one-by-one for endpoints such as growth or lifespan. Given the antimicrobial activity of nanosilver and the fact that antibiotics can extend the lifespan of *C. elegans* cultured by this method (Garigan *et al.*, 2002), we instead utilized liquid axenic media for this study. The use of liquid culture along with microfluidics technology also allowed us to analyze the growth of thousands of *C. elegans* per treatment condition instead of a few dozen as is common with standard techniques (Sprando *et al.*, 2009). For the purpose of developing a panel of assays to evaluate potential nanomaterial toxicity, silver particles of 10-nm diameter (10nmAg) were chosen as a test material for exploratory work. Oxidative damage to DNA was assessed using gas chromatography/tandem mass spectrometry. Additional endpoints of toxicity assessed in this study included 10nmAg uptake and distribution, and morphological changes.

Materials and Methods

Reagents and Test Materials

Nanosilver (10 nm; concentration of 1 mg ml⁻¹ in citrate buffer) was purchased from NanoComposix, Inc. (San Diego, CA, USA). Endotoxin contamination was measured by the manufacturer using a kinetic turbidity assay with endotoxin detection sensitivities of 0.001 EU ml⁻¹ in diluted samples. The absence or presence of endotoxin was confirmed via the gel clot assay (Pyrosate LAL Kit; Associates of Cape Cod Inc., East Falmouth, MA, USA) using both negative (LAL-free water) and positive (endotoxin-spiked samples) controls. Control standard endotoxin was purchased from Associates of Cape Cod, Inc.. ReagentPlus grade silver acetate was purchased from Sigma-Aldrich (St. Louis, MO, USA).

***Caenorhabditis elegans* Culture and Dosing**

The *Caenorhabditis* Genetics Center, which is funded by the NIH National Center for Research Resources, provided the *C. elegans* wild-type N2 Bristol strain used in these experiments. Worm cultures were maintained in **C. elegans** habitation medium (CeHM), an axenic liquid culture media containing *C. elegans* habitation reagent (CeHR) (Rao *et al.*, 2005) and non-fat cows' milk (Sprando *et al.*, 2009), in vented tissue culture flasks and maintained in incubators at 20.5 °C on shakers set to 60 rpm. Synchronized cultures of first larval stage (L1) worms were obtained by bleaching gravid adult worms, collecting the eggs and allowing the eggs to hatch in M9 buffer (Nass & Hamza, 2007). At no point have we observed untreated wild-type *C. elegans* grown in liquid culture for less than 2 weeks to be immobile, therefore worms that did not move during 30 s of continuous observation in a microscope were scored as dead. Preparation and dosing of *C. elegans* larvae was conducted as previously described (Hunt *et al.*, 2012; Sprando *et al.*, 2009). Briefly, nanosilver and equimolar silver in the form of silver acetate (1.55 mg ml⁻¹ silver acetate in water provides 1 mg ml⁻¹ Ag⁺ ions) were diluted in water to 2× the highest concentration used in each experiment and then mixed in a ratio of 2:3:5 (cows' milk)/(CeHR)/(treatment solution in water or just water for controls).

C. elegans were divided into five experimental groups for this study. The first group (Group 1) was utilized to assess the effect of silver nanoparticles on the growth and development of larvae from the L1 stage; Group 2 assessed the effect of silver ions from silver acetate on the growth and development of L1 larvae; Group 3 assessed the effects of silver nanoparticles or silver ions on DNA integrity; Group 4 assessed the effect of purified endotoxin on the growth and development of L1 larvae; Group 5 assessed the effect of endotoxin-free silver nanoparticles in the presence of purified endotoxin on the growth and development of L1 larvae; and Group 6 assessed the effect on the morphology of adult *C. elegans* treated from the second larval (L2) stage of exposure to endotoxin-free silver nanoparticles vs. silver nanoparticles contaminated with endotoxin during manufacture. Group 1 nematodes were exposed for three consecutive days from L1 to 0, 1, 5, 10, 25 and 50 µg ml⁻¹ of endotoxin-free 10nmAg nanoparticles. Group 2 were exposed under identical conditions to 0, 1, 5, 10, 25 and 50 µg ml⁻¹ of silver ions from silver acetate. Group 3 were exposed for 7 or 24 h from the third larval stage to 0, 10 or 50 µg ml⁻¹ of silver nanoparticles or 50 µg ml⁻¹ of silver ions. Group 4 were exposed for three consecutive days from L1 to 0, 10, 25, 50, 100 and 200 Eu ml⁻¹ of purified endotoxin. Group 5 was used to assess the effects on *C. elegans* larval growth from combined exposure of purified endotoxin and nanosilver. Group 5 nematodes were divided into five experimental dose groups and exposed for three consecutive days to both 10nmAg at a concentration of 50 µg ml⁻¹ and increasing concentrations of endotoxin (10, 25, 50, 100 and 200 Eu ml⁻¹). There were two control treatments for Group 5: the first control group was not exposed to either test article, whereas the second control group was exposed to nanosilver at a concentration of 50 µg ml⁻¹ but not endotoxin. Group 6 was treated for three consecutive days from L2 with 0, 10, 25 or 50 µg ml⁻¹ of either endotoxin-free silver nanoparticles or silver nanoparticles contaminated with endotoxin during manufacture.

COPAS Analysis of Growth

The mean COPAS Biosort™ (Complex Object Parametric Analyzer and Sorter; Union Biometrica, Holliston, MA, USA) values for the time-of-flight (TOF, an indication of axial length) parameter were used to evaluate growth on a minimum of 2500 worms per treatment condition per experiment. GP Control Particles (Union Biometrica) were utilized to calibrate the sample pressure so that 15–20 particles pass the sensors per second, and this pressure of 4.95 instrument specific units was utilized in all experiments. Treated *C. elegans* cultures were washed 3 times in M9 (Brenner, 1974) prior to assessment. To distinguish data from background noise, cutoff points for the gating of COPAS data were assessed empirically using the COPAS selection feature (Hunt *et al.*, 2012). Using just hatched L1 *C. elegans*, worms were selected by the COPAS at TOF values of 30 instrument specific units and above, indicating that values below 30 are detections of crystals, bubbles or other elements in the media. Using a control culture after 3 days of post-L1 growth, 8 to 10 worms were selected when sorting for 5 units with TOF values above 800, indicating that readings above 800 were actually measuring multiple *C. elegans* passing the sensors simultaneously. Therefore, all COPAS analyzes were limited to readings with TOF values of 30 to 800 inclusive.

Characterization of 10nmAg in water or CeHM by dynamic light scattering and transmission electron microscopy

Dynamic light scattering (DLS), Zeta potential measurements and transmission electron microscopy (TEM) characterization were performed on the 10nmAg solutions utilized in the study. DLS was performed on a Malvern Zetasizer Nano ZS (Malvern, UK). All cuvettes were triple rinsed with filtered deionized water prior to use. Samples were run at the relevant dosing concentrations. Samples were allowed to equilibrate for 2 min at 25 °C prior to analysis. Analysis was at general resolution with solutions corrected for viscosity and refractive index. Each sample was run in triplicate, with the Zave and polydispersity index (PDI) results presented as an average of the three measurements. Zeta potential measurements were performed on a Malvern Zetasizer Nano ZS, with conditions as noted above, but in pre-rinsed folded capillary cells.

TEM was performed on a JEOL 100CX and a JEOL JEM1400 (JEOL, Japan) at 80 kV. Grids were prepared by dropping 15–20 µl of sample solution onto a holey carbon-coated copper grid. For dilute samples, a second drop of sample was applied to allow for sufficient particle loading for measurement. At least 5 images were taken for each sample, and all particles in frame (~20–60) were measured.

Evaluation of nanosilver uptake and distribution in *C. elegans*

For inductively coupled plasma mass spectroscopy (ICP-MS) measurements, *C. elegans* were treated for 3 days from the L1 stage. For each condition, 5 replicate flasks containing 10 000 *C. elegans* each were pelleted and washed three times in M9 buffer, and then frozen at –20° C for subsequent evaluation. Pellets were digested in PFA vessels with 2 ml of nitric acid in a Milestone Ultraclave (Milestone Inc., Shelton, CT, USA) microwave digestion system (digestion program: 20 min ramp to 200 °C, 20 min hold at 200 °C). Next, 0.5 ml of 10% (volume fraction) HCl

was added to digested samples followed by dilution to 50 ml with DI water. Samples were analyzed for total silver using an Agilent 7500ce ICP-MS (Agilent Technologies, Santa Clara, CA, USA). Data were collected for silver at m/z 107 using Pd as an internal standard.

Distribution of 10nmAg in treated and control worms was analyzed using confocal microscopy. Treated and control worms placed on agar-coated glass slides were anesthetized with sodium azide and observed using a Leica TCS SP5 II confocal microscope (Leica Microsystems, Wetzlar, Germany). All reflection and bright-field images were captured at identical settings. From these images, individual worms were outlined in ImageJ (National Institutes of Health, USA) for size analysis, and then the corresponding region in the reflection image was analyzed for mean pixel intensity within the area of the worm body. For every image, a background value was obtained for a similar area. Background subtraction was deemed unnecessary as in all images background mean pixel intensity values (measured at 0.008 to 0.012) were less than 10% of the average control mean pixel intensity of 0.192 (ImageJ specific units).

Total DNA extraction from *C. elegans*

The extraction of DNA from *C. elegans* was based on the previously published and validated protocols of Meyer and colleagues (Boyd *et al.*, 2010b; Meyer, 2010; Meyer *et al.*, 2010). These protocols, which utilize freezing and grinding of *C. elegans* in liquid nitrogen, have been shown to minimize excess oxidation of DNA even although some low level of background oxidation is to be expected. However, the nominal background oxidation level can be accounted for through the use of proper controls during both DNA extraction and DNA analysis (Rodriguez *et al.*, 2000). Briefly, after exposure, *C. elegans* were washed three times in M9 to remove residual exposure medium, and centrifuged to form a pellet. *C. elegans* pellets were frozen in liquid nitrogen, crushed in a liquid nitrogen cooled cryopulverizer, ground in a liquid nitrogen cooled cell crusher and subsequently dissolved in G2 buffer and homogenized in a dounce homogenizer using 5 strokes each of loose and tight fitting plungers. Lysed worm bodies were treated with RNase A (Qiagen, Venlo, Netherlands) then digested by proteinase K (Qiagen). Residual debris was removed by centrifugation and the DNA was isolated from the resultant supernatant using Qiagen Gene-tip columns following the manufacturer's suggested protocols for loading, washing and elution. Isolated DNA was precipitated with the subsequent addition of saturated sodium chloride and ice-cold absolute ethanol. DNA pellets were washed three times with ice cold 70% (volume fraction) ethanol and once with ice-cold absolute ethanol to remove residual salts. The clean DNA pellets were dried under Speed Vac and stored at -20°C with desiccant until analysis by mass spectrometry.

Gas chromatography/tandem mass spectrometry (GC/MS/MS) measurement of oxidatively induced DNA damage

Isotope-dilution GC/MS/MS determination of oxidatively modified DNA bases (DNA lesions) in *C. elegans* DNA extracts using multiple reaction monitoring (MRM) mode quantification was conducted based on modifications to the selected ion monitoring (SIM) mode gas chromatography/mass spectrometry (GC/MS) methodology originally developed at NIST (Dizdaroglu, 1984, 1985; Dizdaroglu *et al.*, 2002). In the current MRM mode methodology, specific reaction transitions for nine lesions

[4,6-diamino-5-formamidopyrimidine (FapyAde), 2,6-diamino-4-hydroxy-5-formamidopyrimidine (FapyGua), 8-hydroxyguanine (8-OH-Gua), 8-hydroxyadenine (8-OH-Ade), 5-hydroxycytosine (5-OH-Cyt), thymine glycol (TG), 5-hydroxyuracil (5-OH-Ura), 5-hydroxy-5-methylhydantoin (5-OH-5-MeHyd), 5-hydroxymethyluracil (5-OH-MeUra)], as well as for their stable isotopically-labeled analogues (FapyAde- ^{13}C , $^{15}\text{N}_2$, FapyGua- ^{13}C , $^{15}\text{N}_2$, 8-OH-Gua- $^{15}\text{N}_5$, 8-OH-Ade- ^{13}C , $^{15}\text{N}_2$, 5-OH-Cyt- ^{13}C , $^{15}\text{N}_2$, TG-d $_4$, 5-OH-Ura- $^{13}\text{C}_4$, $^{15}\text{N}_2$, 5-OH-5-MeHyd- ^{13}C , $^{15}\text{N}_2$ and 5-OHMeUra- $^{13}\text{C}_2$, d $_2$) were identified and optimized on the basis of the original SIM ions. The isotopically-labeled lesion analogs function as internal standards (ISTDs) for lesion quantification. Additional details regarding the GC/MS/MS methodology and instrumental details can be found in the supplemental section. Brief enzymatic hydrolysis and analysis details for the extracted *C. elegans* DNA pellets follow (all analyzes were conducted using six biologically independent samples). DNA pellets were re-dissolved in distilled, deionized water (ddH $_2$ O) and the DNA concentration was determined by spectrophotometric absorbance at 260 nm (absorbance of 1 = 50 μg of DNA per ml). Sample aliquots containing 50 μg DNA were prepared from each *C. elegans* extract and the nine lesion ISTDs were added to each sample. The samples were dried under vacuum and then stored at 4°C prior to enzymatic digestion. Subsequent to enzymatic digestion, samples were dissolved in a buffer consisting of 50 mmol l^{-1} sodium phosphate, 100 mmol l^{-1} potassium chloride, 1 mmol l^{-1} EDTA and 100 $\mu\text{mol l}^{-1}$ dithiothreitol (pH 7.4). To this solution, 2 μg each of *E. coli* formamidopyrimidine DNA glycosylase - Fpg (Trevigen) and *E. coli* endonuclease (III) - EndoIII (Trevigen) were added and the sample was digested at 37°C for 1 h. Hydrolysis using these enzymes prevents artifactual formation of DNA lesions because it only releases modified bases; consequently, there is no intact DNA nor unmodified base present during the trimethylsilylation step. The digestion was terminated with the addition of ice-cold absolute ethanol in combination with sample storage at -20°C . Samples were centrifuged at 14 000 g for 30 min, supernatant fractions containing the excised DNA lesions were transferred to glass vials and the solvent was removed under Speed Vac. Samples were solubilized in ddH $_2$ O, lyophilized, and then trimethylsilylated using bis(trimethylsilyl)trifluoroacetamide / 1% trimethylchlorosilane in pyridine (120°C for 30 min). After derivatization, samples were analyzed by GC/MS/MS and the final results were reported in terms of the number of lesions quantified / 10^6 DNA bases.

Statistical analysis of DNA lesions were conducted using Graphpad Prism software (Graphpad Software Inc., La Jolla, CA, USA). Outliers were removed using Grubb's outlier test and accounted for ~5% of the data collected. Data from different conditions were compared using ANOVA followed by Dunnett's test when multiple conditions were examined or Student's t-test when comparing two conditions ($\alpha = 0.05$).

Results

Physicochemical properties of 10nmAg in water or CeHM

All silver samples tested in water by DLS were ~14–16 nm in diameter (Zave) with a PDI of 0.15–0.17. Zeta potentials ranged from -42 to -48 mV (Fig. 1A). TEM analysis indicated that the particles in water were roughly spherical (Fig. 1B) with an average diameter of ~8–9 nm. A wide particle size distribution was noted, with both larger (> 20 nm) and smaller particles

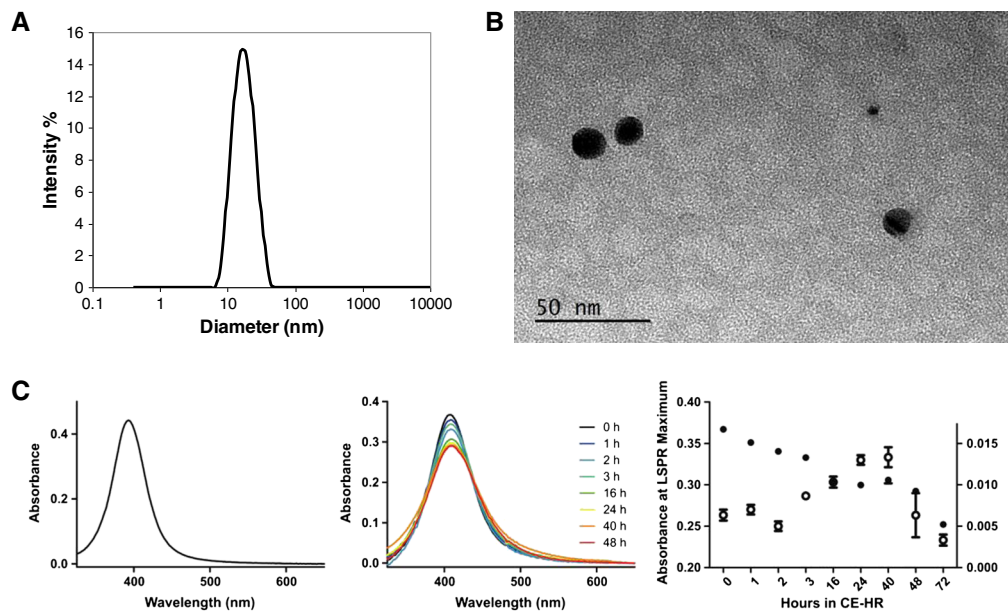


Figure 1. Silver nanoparticle characterization. (A) Representative intensity-weighted dynamic light scattering (DLS) measurement of 10nmAg dispersed in water, showing a single peak centered around ~15 nm. (B) Representative transmission electron microscopy (TEM) of 10nmAg dispersed in water. Particles were generally dispersed as primary particles and were roughly spherical in shape. (C) 10nmAg stability in *C. elegans* habitation medium (CeHM). Left panel: initial UV-Vis absorption spectrum of 10nmAg as received ($50 \mu\text{g ml}^{-1}$). Middle panel: monitoring of $50 \mu\text{g ml}^{-1}$ 10nmAg stability in CeHM over 48 h. Exposure conditions were conducted up to 24 h in culture (yellow absorption peak) showing decreased localized surface plasmon resonance (LSPR) absorption but little evidence of particle agglomeration. Right panel: comparison of LSPR maximum absorption (dark circles, left Y-axis) to absorption at 550 nm (white circles, right Y-axis). Uncertainties are standard deviations ($n \geq 3$).

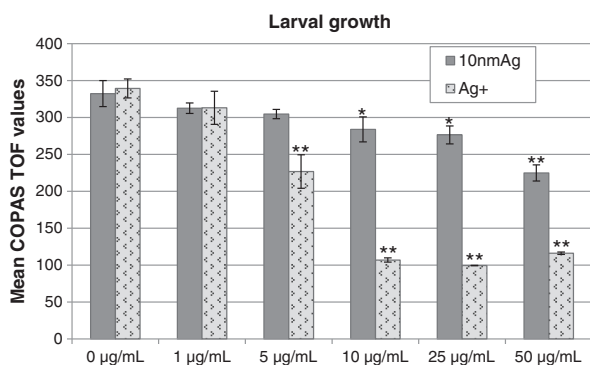


Figure 2. Ten nanometer silver particles (10nmAg) inhibit the growth of *Caenorhabditis elegans* larvae, but not as strongly as ionic silver (Ag^+). 10nmAg at concentrations of $10 \mu\text{g ml}^{-1}$ and above inhibit the growth of *C. elegans* larvae, as indicated by reduced mean COPAS (Complex Object Parametric Analyzer and Sorter) TOF (time-of-flight) values (dark gray bars). Ag^+ from silver acetate (hatched bars) had a greater effect on growth than 10nmAg. Bars represent means \pm standard deviation from each of three replicates. Each COPAS test replicate evaluated a minimum of 2500 animals. * $P < 0.05$, ** $P < 0.005$, as compared by the *t*-test to the $0 \mu\text{g ml}^{-1}$ control.

(< 5 nm) present. We were unable to use DLS sizing of particles dispersed in CeHM, the axenic liquid growth media utilized in these experiments, as the media itself had protein peaks in the same size range as the 10nmAg. TEM analysis indicated that the 10nmAg in CeHM substantially remained as primary particles, with little agglomeration noted upon addition to the media. UV/VIS analysis (Fig. 1C) further suggested that 10nmAg are stabilized by protein adsorption in CeHM (Supplementary Information). This

stability is most probably due to protein opsonization on the surface of the 10nmAg. Such stabilization has been noted in culture media for other noble metal nanoparticles (Keene & Tyner, 2011).

Exposure to 10nmAg inhibits the growth of *C. elegans* larvae

The COPAS Biosort™ system automates the analysis, sorting and dispensing of hundreds of nematodes per minute. The time-of-flight, or TOF, parameter is an indication of length. Mean TOF values steadily increase as *C. elegans* develop from larvae to adult (Sprando *et al.*, 2009). The growth and development of the control worms were similar to that previously reported by our laboratory (Sprando *et al.*, 2009), whereas mean COPAS TOF values obtained in triplicate from a minimum of 2500 worms per replicate indicated that 10nmAg at 10, 25 and $50 \mu\text{g ml}^{-1}$ reduced the axial length by 15%, 17% and 32%, respectively (Fig. 2, dark gray bars). Length differences at 1 and $5 \mu\text{g ml}^{-1}$ were not statistically significant. Using nanoparticle-free supernatant obtained by centrifuging 10nmAg nanoparticles for 5 h at RFC 65 800 *g* at a volume equal to that used to obtain the $50 \mu\text{g ml}^{-1}$ 10nmAg treatment condition, we found no change in growth relative to controls (data not shown), suggesting that soluble impurities were not the cause of growth inhibition.

Ionic silver is more toxic to *C. elegans* larvae than 10nmAg

Silver ions (Ag^+) from silver acetate had a much greater effect on growth than the 10nmAg, with 5 and $10 \mu\text{g ml}^{-1}$ Ag^+ reducing the axial length by 33% and 68%, respectively (Fig. 2, hatched bars). Increased concentrations of 25 and $50 \mu\text{g ml}^{-1}$ Ag^+ did

not further reduce growth, however most of the $10\ \mu\text{g ml}^{-1}$ Ag^+ treated *C. elegans* were still alive and moving, whereas about half of those treated with $25\ \mu\text{g ml}^{-1}$ Ag^+ were not moving and assumed dead (data not shown). Nearly all of the observed worms treated with $50\ \mu\text{g ml}^{-1}$ Ag^+ appeared to be dead (Fig. S1).

Uptake and localization of 10nmAg in *C. elegans*

Excitation of surface plasmons and reflection of light by nanosilver aggregates allowed us to investigate the uptake and distribution of 10nmAg in *C. elegans* by confocal microscopy (Akimov et al., 2007). If reflection was observed in controls, it was usually found at very low levels in the grinder region of the posterior pharyngeal bulb (Fig. 3A). In *C. elegans* treated for 3 days from the first larval stage with $10\ \mu\text{g ml}^{-1}$ of 10nmAg, reflective punctate structures were observed, mostly in the lumen and tissues of the pharynx and intestine (Fig. 3B). Increasing the 10nmAg concentration to $50\ \mu\text{g ml}^{-1}$ did not appear to increase reflection or alter localization patterns (Fig. 3C, top). Consistent with COPAS TOF findings, *C. elegans* treated with $50\ \mu\text{g ml}^{-1}$ of 10nmAg appeared to be both smaller than controls and at an earlier stage of development (Fig. 3C, middle). We confirmed the size difference at $50\ \mu\text{g ml}^{-1}$ 10nmAg by measuring the relative whole body area of each worm from images using ImageJ software (Fig. 4A, light gray bars). We also measured pixel

intensity over the area of the whole worm body and found similar increases in pixel intensity at 10 and $50\ \mu\text{g ml}^{-1}$ 10nmAg, indicating a limit to the uptake of 10nmAg (Fig. 4A, dark gray bars). These results were confirmed by ICP-MS analysis, which found similar levels of silver in *C. elegans* treated with 10 and $50\ \mu\text{g ml}^{-1}$ of 10nmAg for 3 days from L1 (Fig. 4B, dark gray bars). Silver uptake after treatment with $10\ \mu\text{g ml}^{-1}$ Ag^+ from silver acetate was comparable to 10nmAg (Fig. 4B, hatched bars). However, *C. elegans* larvae treated with $50\ \mu\text{g ml}^{-1}$ Ag^+ had far lower levels of silver uptake than those treated with $50\ \mu\text{g ml}^{-1}$ 10nmAg. This is probably due to the fact that most of the *C. elegans* from the $50\ \mu\text{g ml}^{-1}$ Ag^+ treatment populations were dead before the experiment was completed.

Exposure to 10nmAg induces oxidative damage to DNA in *C. elegans*

Third larval stage *C. elegans* were exposed to 10nmAg or Ag^+ in CeHM for 4 or 24 h. Subsequent to freezing in liquid nitrogen, DNA was extracted and DNA lesion formation and accumulation was assessed via GC/MS/MS analysis (Supplementary Methods). Four-hour exposure yielded no evidence of increased DNA damage, but 24-h exposure to $10\ \mu\text{g ml}^{-1}$ 10nmAg produced a 75% increase in the levels of 8-OH-Gua (Fig. 5). 8-OH-Gua is an established biomarker of oxidative stress and a mutagenic lesion

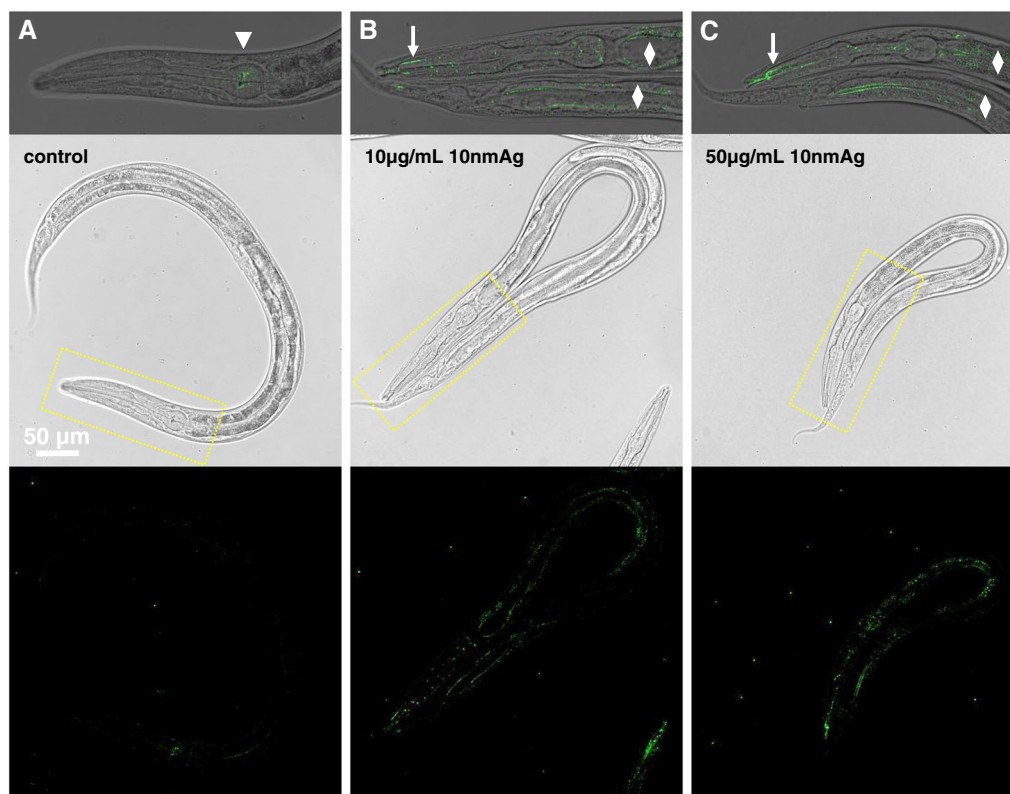


Figure 3. Confocal reflection analysis of developing larvae indicates 10nmAg concentration in pharyngeal and intestinal tissues. (A) Very low levels of reflection are detected in the grinder of the posterior pharyngeal bulb (arrowhead) in control day-3 post-L1 *C. elegans*. (B) Treatment with $10\ \mu\text{g ml}^{-1}$ 10nmAg is associated with a large increase in reflective puncta clustered in pharyngeal (arrow) and intestinal (diamonds) tissues. (C) *C. elegans* treated with $50\ \mu\text{g ml}^{-1}$ 10nmAg have similar overall brightness and localization patterns of reflection as those treated with $10\ \mu\text{g ml}^{-1}$. However, consistent with COPAS (Complex Object Parametric Analyzer and Sorter) TOF (time-of-flight) data, observed worms in this treatment group were smaller than the controls, with less developed gonadal structures (asterisk). Top: overlay of the head or head and tail region outlined in yellow on the brightfield image; Middle: confocal brightfield image; Bottom: the same field detecting reflected light.

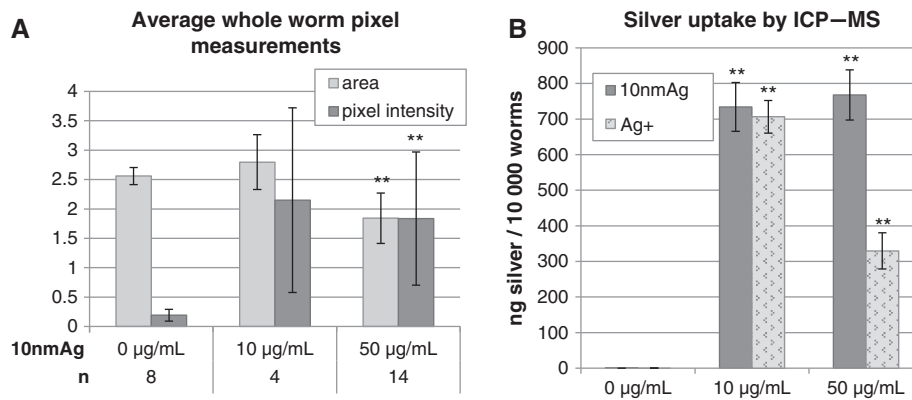


Figure 4. Analysis of silver uptake in *C. elegans*. (A) ImageJ analysis of whole worm relative size (area) and pixel intensity from confocal brightfield and reflection images indicates a decrease in the size of *C. elegans* larvae treated with 50 µg ml⁻¹ 10nmAg, and similar increases in reflection in those treated with 10 and 50 µg ml⁻¹ 10nmAg. Bars represent means ± standard deviations (SD) of the relative area or pixel intensity over the whole worm body. 10nmAg concentration and the number of individuals evaluated is indicated. (B) ICP-MS analysis of silver uptake in *C. elegans* after 3 days of larval treatment with 10nmAg or Ag⁺ at 0, 10 and 50 µg ml⁻¹. Bars represent means ± standard deviation (SD) of the mass of silver (ng) in 10 000 triple-washed worms from each of five samples per treatment. ***P* < 0.005, as compared by the *t*-test to the 0 µg ml⁻¹ control.

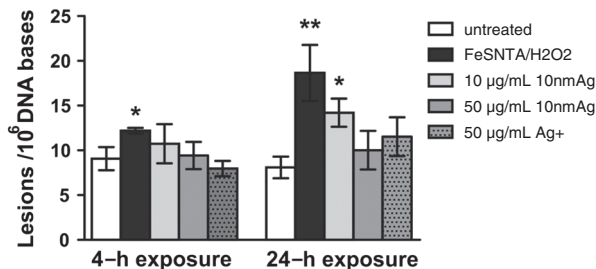


Figure 5. Formation of 8-OH-Gua in *Caenorhabditis elegans* exposed to 10nmAg. 8-OH-Gua levels were measured at two different exposure time points. Iron II sulfide–nitrotriacetic acid / hydrogen peroxide (FeSNTA/H₂O₂) reagent was used as a positive control for DNA damage and generated increased lesion levels at both 4- and 24-h exposures. 10nmAg exposure resulted in increased 8-OH-Gua levels after 24 h at 10 µg ml⁻¹, but not the 50 µg ml⁻¹ concentration, whereas Ag⁺ exposure did not result in increased oxidative DNA lesion levels. Asterisks indicate statistically significant results compared with the untreated samples using one-way analysis of variance (ANOVA) followed by Dunnett's multiple comparison test. One or two asterisks indicate *P* < 0.05 or *P* < 0.01, respectively. All data represents the mean of six independent measurements. Uncertainties are standard deviations.

causing G → T transversion mutations (Cooke *et al.*, 2003). Interestingly, neither 50 µg ml⁻¹ Ag⁺ from silver acetate nor 50 µg ml⁻¹ of 10nmAg induced the accumulation of lesions whereas they both exhibited strong signs of toxicity as indicated by inhibited growth.

Endotoxin contamination of 10nmAg associated with increased toxicity

An unexpected finding of this study was that some lots of 10nmAg from the same manufacturer were more toxic than others (Fig. 6A). 10nmAg lots with increased toxicity were later identified by the manufacturer as containing 22 Eu ml⁻¹ endotoxin. All 10nmAg lots were then tested in house by the gel clot assay, and results confirmed the manufacturer's assessment of endotoxin status. In an effort to understand the contributing factors to increased toxicity, we tested the

growth of *C. elegans* in the presence of 0 to 200 Eu ml⁻¹ of purified endotoxin and found no effect on growth (Fig. 6B) or morphology (data not shown). We then tried mixing 0 to 200 Eu ml⁻¹ of purified endotoxin with 50 µg ml⁻¹ of 10nmAg and again found no difference in growth inhibition with or without endotoxin (Fig. 6C). Comparison of DLS, Zeta potential measurements and TEM analyzes for the endotoxin-free and endotoxin contaminated 10nmAg lots indicated that they were similar in composition (Fig. 7).

ICP-MS analysis indicated that endotoxin status of individual 10nmAg lots did not influence uptake levels (data not shown). However, the presence of endotoxin contamination of 10nmAg did have a strong effect on vulval morphology in *C. elegans*. We observed no protruding vulva in 150 control adult *C. elegans* (Fig. 8A–C), and very few in those treated with endotoxin free lots of 10nmAg for 3 days from L2. In contrast, over half of the *C. elegans* treated for 3 days from L2 with 50 µg ml⁻¹ endotoxin contaminated 10nmAg had protruding vulva (Fig. 8A, D and E). In some animals with gross vulval abnormalities, retained eggs hatched inside the parent. This may be an adaptive response to stressful conditions, allowing progeny to consume the parent from within and develop inside the protected environment of the adult cuticle, as is known to occur in low nutrient environments (Chen & Caswell-Chen, 2004). It is important to note that observations of confocal reflection in the pharynx of internally hatched larvae (Fig. 8E, arrow) do not necessarily indicate tissue transfer of nanosilver through the adult intestine, pseudocoelom and uterus, to developing progeny. Rather, localization of nanosilver to internally hatched larvae may be due to matrotrophy, or to nanosilver entry into the uterus from the environment through the damaged vulva.

At this point, we had exhausted our supply of the endotoxin contaminated 10nmAg and the manufacturer could not supply us with additional material from the same lot. We were therefore unable to identify the specific component(s) which had induced the higher level of toxicity. While our data is incomplete, we feel that it is important to report the data we have as it indicates that findings of nanomaterial toxicity in the absence of endotoxin testing may be due to the presence of contaminants rather than the nanomaterial.

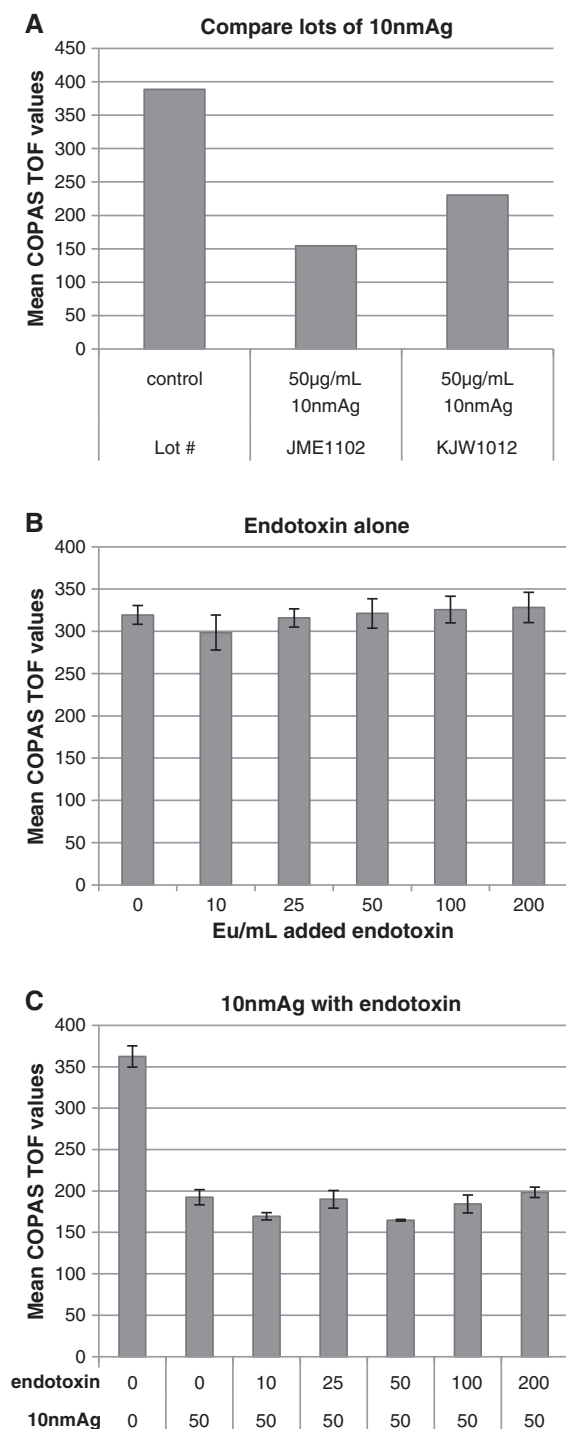


Figure 6. Endotoxin contamination of 10nmAg was associated with increased toxicity. (A) 10nmAg that was later discovered to contain 22 Eu ml⁻¹ endotoxin, represented here by lot# JME1102, had a greater effect on *Caenorhabditis elegans* growth than endotoxin-free preparations. (B) Purified endotoxin did not reproduce the growth inhibition effect of endotoxin-contaminated 10nmAg. (C) Adding 0 to 200 Eu ml⁻¹ purified endotoxin to 50 µg ml⁻¹ 10nmAg (endotoxin concentration in Eu/ml, and 10nmAg concentration in µg/ml on the bottom row) also did not alter the growth response. Bars in (A) represent the means from single samples evaluating COPAS (Complex Object Parametric Analyzer and Sorter) TOF (time-of-flight) for a minimum of 2500 animals per sample, bars and error bars in (B) and (C) represent means \pm standard deviation (SD) from each of three replicates.

Discussion

In spite of the rapid growth of nanomaterial-containing consumer products available, there is limited information on the interaction of nanomaterials with biological systems or the potential health ramifications of exposure (Asharani *et al.*, 2008; Laboratory, 2010; Nel *et al.*, 2006). Available data on nanomaterial toxicity come from a variety of different model systems utilizing small numbers of specific nanomaterial types, making it difficult to compare data from one study to another. In order to improve nanomaterial risk characterization, there is a need for the development of standardized rapid screening protocols to assess the toxicity of nanoparticles. As nanosilver is the fastest growing category of nanomaterial on the market (Fabrega *et al.*, 2011; Wijnhoven *et al.*, 2009), we utilized 10nmAg as a model nanomaterial to evaluate the utility of rapid nanomaterial toxicity assays in *C. elegans* for growth, tissue distribution, DNA damage and morphology.

In several published studies, nanosilver has demonstrated similar or enhanced antibacterial activity relative to silver ions (Choi & Hu, 2009; Fabrega *et al.*, 2009; Lok *et al.*, 2006; Sotiriou & Pratsinis, 2010). We found that 10nmAg was far less toxic than ionic silver to *C. elegans* larvae. This is consistent with a recent report which found reduced body weight gain in rats treated with silver acetate but not in those treated with 14-nm polyvinylpyrrolidone-coated nanosilver (Hadrup *et al.*, 2012). We also found that 10nmAg induced mild dose-dependent growth suppression at concentrations of 10 µg ml⁻¹ and above. This finding is consistent with a recent *in vitro* study which found that 10nmAg was associated with slight but significant dose-dependent decreases in the viability of adipogenic stem cells at 10, 50 and 100 µg ml⁻¹ (Samberg *et al.*, 2012). Taken together, these findings suggest the possibility that in comparing nanosilver and ionic silver, the equally or potentially more effective antibacterial agent is the less toxic one, and that as a model for toxicity screening, *C. elegans* may have potential in predicting nanomaterial toxicity ranking for mammals.

We used confocal reflection analysis to infer nanosilver localization (Akimov *et al.*, 2007) within *C. elegans*. Very little if any reflection was observed in untreated worms, whereas those treated with either 10 or 50 µg ml⁻¹ of 10nmAg had similarly high levels of reflection in digestive tract tissues. It must be noted that nanosilver distribution in both zebra fish (*Danio rerio*) and rats after environmental and oral application, respectively, indicated extensive transport to multiple tissues including the brain (Asharani *et al.*, 2008; Loeschner *et al.*, 2011). Thus, it may be that vertebrate models will be better predictors of nanomaterial distribution and damage to specific human organs or tissues. Additionally, given biological and methodological constraints, it is unlikely that *C. elegans* will prove useful in predicting safe vs. toxic dose levels for humans. However, the goal of large-scale, rapid toxicity screening is to identify potentially harmful compounds for further investigation. Significant correlations between toxicity ranking in rat and *C. elegans* have been found (Boyd *et al.*, 2010a; Cole *et al.*, 2004; Ferguson *et al.*, 2010; Hunt *et al.*, 2012; Williams & Dusenbery, 1988), and with this work, we have identified correlations between responses to nanosilver exposure among rat, cell culture and *C. elegans* models. Thus, a 3-day *C. elegans* larval growth screen with the potential to identify nanomaterials likely to cause harm to humans and the environment may be useful in determining how best to allocate limited funding for further, more in-depth risk evaluation.

Sample	AgNP Concentration	Endotoxin level	Zave diameter (nm)	sd	Zeta Potential	sd	PDI	TEM diameter (nm)	TEM Notes
Endotoxin (-)	50 $\mu\text{g}/\text{mL}$	< 2.5 EU/mL	16.2	0.17	-41.6	2.56	0.152	9.2	Dispersed with both larger and smaller particles present. TEM size based on 19 measured particles.
Endotoxin (+)	10 - 50 $\mu\text{g}/\text{mL}$	22 EU/mL	13.7	0.1	-48	2	0.17	8.0	Dispersed with both larger and smaller particles present. TEM size based on 61 measured particles.

Figure 7. Summary of characterization of endotoxin-free and endotoxin-contaminated 10nmAg by dynamic light scattering (DLS), Zeta potential measurements and transmission electron microscopy (TEM).

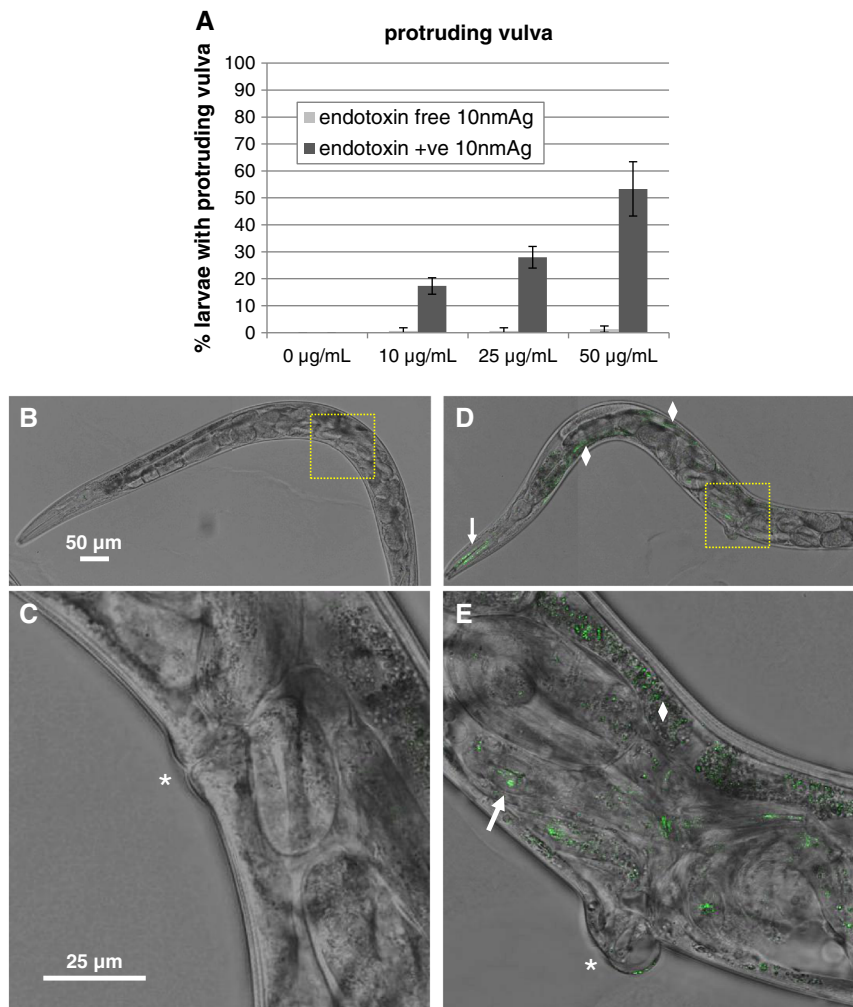


Figure 8. Endotoxin positive lots of 10nmAg were associated with vulval abnormalities and internal hatching in *Caenorhabditis elegans*. (A) After a 3-day treatment beginning at L2 with 0 to 50 $\mu\text{g ml}^{-1}$ 10nmAg with and without endotoxin contamination, fifty larvae were evaluated for vulval morphology from each of three replicate flasks for each treatment. Bars represent means \pm standard deviation (SD) of the percent of *C. elegans* with protruding vulva. (B) Very low levels of reflection were detected by confocal microscopy in control adult *C. elegans*. (C) The enlarged region from (B) shows normal vulval morphology (asterisk). (D) Confocal reflection in adult *C. elegans* after 3 days of treatment from the second larval stage with 50 $\mu\text{g ml}^{-1}$ endotoxin-contaminated 10nmAg was mostly confined to the pharynx (arrow) and intestine (diamonds). Endotoxin contamination of 10nmAg was associated with protruding vulva and internal hatching. (E) Enlarged region from (D) shows a grossly abnormal vulva (asterisk), and reflection in both the parental intestine (diamond) and in retained hatched larvae (arrow). Yellow dotted squares indicate enlarged regions.

Oxidatively generated DNA lesions may arise as a result of imbalance in the redox environment of the cells and are critically important to understanding the genotoxic potential of nanomaterials (Petersen & Nelson, 2010). This damage can lead to a variety of genotoxic outcomes such as DNA strand

breaks, gene miss-translation and mutations (Cooke *et al.*, 2003). In humans, oxidatively generated lesions accumulate in a number of disease states including cancer, Alzheimer's disease (Tuna *et al.*, 2011), atherosclerosis (Jaruga *et al.*, 2012) and others (Evans *et al.*, 2004). The identification and quantitative

determination of DNA lesions using mass spectrometry-based techniques is a promising alternative to assays widely used in molecular toxicology, such as the Ames test or comet assay, which have been confounded by artifacts arising from DNA-nanoparticle interactions in previous nanotoxicology studies (Karlsson, 2010; Rajapakse *et al.*, 2012; Lin *et al.*, 2009).

Nanosilver exposure has been associated with chromosomal aberrations and DNA damage in mammalian cell cultures (Asharani *et al.*, 2009a, 2009b; Foldbjerg *et al.*, 2011; Mei *et al.*, 2012). We found that 10nmAg at $10 \mu\text{g ml}^{-1}$ after a 24-h exposure resulted in significantly increased 8-OH Gua levels. This highly mutagenic lesion is found at elevated levels in patients with various cancers and degenerative disorders (Cooke *et al.*, 2003). Neither $50 \mu\text{g ml}^{-1}$ of 10nmAg nor $50 \mu\text{g ml}^{-1}$ Ag^+ produced oxidative damage, although both treatments clearly inhibited growth. There are a number of hypotheses for why this effect was observed. One possible explanation is that worms with inhibited development are more resistant to DNA damage. Previous studies have demonstrated that *C. elegans* DNA repair processes decline with development, and inhibited development may stall worms at an early stage with more active DNA repair (Meyer *et al.*, 2007). Alternatively, the chromatin in the developing *C. elegans* germ line of late stage larvae may provide a pool of DNA that is more vulnerable to oxidative damage. If this is the case, then the DNA damage may not be seen at $50 \mu\text{g ml}^{-1}$ of 10nmAg or Ag^+ because these animals are still at an earlier stage of gonadal development.

Endotoxin, or lipopolysaccharide, is a component of bacterial cell walls. We found that endotoxin contamination of some 10nmAg lots was associated with vulval protrusion, retention of eggs, and internal hatching. As *C. elegans* larvae that hatch internally are known to consume parental tissues (Chen & Caswell-Chen, 2004), detection of 10nmAg in internally hatched larvae may be the result of matrotrophy. Alternatively, environmental nanosilver may be able to enter the uterus via the damaged vulva. Thus, nanosilver localization to internally hatched larvae cannot necessarily be taken to indicate tissue transfer to progeny. Our published (Hunt *et al.*, 2012) and unpublished observations (data not shown) suggest that vulval abnormalities and retained eggs are a *C. elegans* response to many different types of toxins. It has been proposed that facultative vivipary, in which the progeny consume the parent from the inside, is an adaptive strategy for species survival in cyclical low nutrient environments (Chen & Caswell-Chen, 2004). To this theory, we add the idea that the same or similar genetic mechanisms may be activated in *C. elegans* in the presence of some toxins, providing progeny with an opportunity to develop inside the protected environment of the parental cuticle.

We also found that endotoxin contaminated lots of 10nmAg had a greater adverse effect on *C. elegans* larval growth than endotoxin-free preparations, stressing the need for endotoxin testing of all nanomaterials. We did not observe an effect on larval growth or morphology after exposing *C. elegans* larvae to purified endotoxin, nor did pre-incubating endotoxin-free 10nmAg with purified endotoxin appear to increase toxicity, supporting the proposition that detection of endotoxin in sterile nanomaterial preparations may act as a marker for the presence of other unidentified contaminants introduced during nanomaterial synthesis (Oostingh *et al.*, 2011).

Conclusion

Exposure to 10nmAg reduced growth and development in *C. elegans* larvae at environmental concentrations of $10 \mu\text{g ml}^{-1}$

and above. Consistent with rat data, 10nmAg was significantly less toxic to *C. elegans* than Ag^+ . Confocal reflection analysis suggests that 10nmAg localized primarily to digestive tissues in *C. elegans*. As previously found in several unrelated studies using mammalian cell cultures, *C. elegans* exposure to 10nmAg induced DNA damage, detected here as increased levels of 8-OH Gua. Together, these findings suggest that screens using *C. elegans* may prove a useful component in risk assessment protocols for nanoparticle toxicity.

SUPPORTING INFORMATION

Additional Supporting Information may be found in the online version of this article.

Acknowledgments

The authors would like to thank Li Ni Komatsu (L.N.K.) for beginning this study, Dr Jeffrey Yourick for careful reading of this manuscript, Dr Dave Sebba of NanoComposix, Inc. for technical assistance in handling silver nanoparticles, and Thomas N. Black and Michael Scott for assistance in preparing media. Author contributions: experimental concept design, R.L.S.; nanoparticle characterization, K.T., B.J.M.; COPAS analysis, P.R.H., NO; confocal reflection, L.N.K., P.R.H.; morphology assessments, P.R.H., L.N.K.; DNA damage, B.J.M., B.C.N.; ICP-MS, S.C., P.R.H.; manuscript preparation, P.R.H., R.L.S., K.T., B.J.M., BCN. Funding Source: United States Food and Drug Administration/Center for Food Safety and Applied Nutrition/Office of Applied Research and Safety Assessment/Division of Toxicology. The funders had no role in study design, data collection and analysis, decision to publish, or preparation of the manuscript. The authors declare there are no conflicts of interest. B.J.M. was supported by a National Research Council associateship provided by the National Academy of Sciences. The findings and conclusions in this article have not been formally disseminated by the Food and Drug Administration and should not be construed to represent any Agency determination or policy. The mention of commercial products, their sources, or their use in connection with material reported herein is not to be construed as either an actual or implied endorsement of such products by the Department of Health and Human Services. Certain commercial equipment, instruments and materials are identified in this paper to specify an experimental procedure as completely as possible. In no case does the identification of particular equipment or materials imply a recommendation or endorsement by the National Institute of Standards and Technology nor does it imply that the materials, instruments, or equipment are necessarily the best available for the purpose.

References

- Ahamed M, Karns M, Goodson M, Rowe J, Hussain SM, Schlager JJ, Hong Y. 2008. DNA damage response to different surface chemistry of silver nanoparticles in mammalian cells. *Toxicol. Appl. Pharmacol.* **233**: 404–410.
- Akimov AV, Mukherjee A, Yu CL, Chang DE, Zibrov AS, Hemmer PR, Park H, Lukin MD. 2007. Generation of single optical plasmons in metallic nanowires coupled to quantum dots. *Nature* **450**: 402–406.
- Alexander JW. 2009. History of the medical use of silver. *Surg. Infect. (Larchmt.)* **10**: 289–292.
- Asharani PV, Hande MP, Valiyaveetil S. 2009a. Anti-proliferative activity of silver nanoparticles. *BMC Cell Biol.* **10**: 65.
- Asharani PV, Lian Wu Y, Gong Z, Valiyaveetil S. 2008. Toxicity of silver nanoparticles in zebrafish models. *Nanotechnology* **19**: 255102.
- Asharani PV, Low Kah Mun G, Hande MP, Valiyaveetil S. 2009b. Cytotoxicity and genotoxicity of silver nanoparticles in human cells. *ACS Nano* **3**: 279–290.

- Avery L, You YJ. 2012. *C. elegans* feeding. *WormBook*: 1–23.
- Berger TJ, Spadaro JA, Chapin SE, Becker RO. 1976. Electrically generated silver ions: quantitative effects on bacterial and mammalian cells. *Antimicrob. Agents Chemother.* **9**: 357–358.
- Bonner JC. 2010. Nanoparticles as a potential cause of pleural and interstitial lung disease. *Proc. Am. Thorac. Soc.* **7**: 138–141.
- Boyd WA, McBride SJ, Rice JR, Snyder DW, Freedman JH. 2010a. A high-throughput method for assessing chemical toxicity using a *Caenorhabditis elegans* reproduction assay. *Toxicol. Appl. Pharmacol.* **245**: 153–159.
- Boyd WA, Crocker TL, Rodriguez AM, Leung MCK, Lehmann DW, Freedman JH, Houten BV, Meyer JN. 2010b. Nucleotide excision repair genes are expressed at low levels and are not detectably inducible in *Caenorhabditis elegans* somatic tissues, but their function is required for normal adult life after UVC exposure. *Mutat. Res.* **683**: 57–67.
- Brenner S. 1974. The genetics of *Caenorhabditis elegans*. *Genetics* **77**: 71–94.
- Chae YJ, Pham CH, Lee J, Bae E, Yi J, Gu MB. 2009. Evaluation of the toxic impact of silver nanoparticles on Japanese medaka (*Oryzias latipes*). *Aquat. Toxicol.* **94**: 320–327.
- Chen J, Caswell-Chen EP. 2004. Facultative Vivipary is a Life-History Trait in *Caenorhabditis elegans*. *J. Nematol.* **36**: 107–113.
- Choi O, Hu Z. 2008. Size dependent and reactive oxygen species related nanosilver toxicity to nitrifying bacteria. *Environ. Sci. Technol.* **42**: 4583–4588.
- Choi OK, Hu ZQ. 2009. Nitrification inhibition by silver nanoparticles. *Water Sci. Technol.* **59**: 1699–1702.
- Cole RD, Anderson GL, Williams PL. 2004. The nematode *Caenorhabditis elegans* as a model of organophosphate-induced mammalian neurotoxicity. *Toxicol. Appl. Pharmacol.* **194**: 248–256.
- Congress. 2000. ICCVAM (Interagency Coordinating Committee on the Validation of Alternative Methods) Authorization Act of 2000 (Public Law 106-545).
- Cooke MS, Evans MD, Dizdaroglu M, Lunec J. 2003. Oxidative DNA damage: mechanisms, mutation, and disease. *FASEB J.* **17**: 1195–1214.
- Dizdaroglu M. 1984. The use of capillary gas-chromatography mass-spectrometry for identification of radiation-induced DNA base damage and DNA base amino acid cross links. *J. Chromatogr.* **295**: 103–121.
- Dizdaroglu M. 1985. Application of capillary gas-chromatography mass-spectrometry to chemical characterization of radiation-induced base damage of DNA : Implications for assessing DNA-repair processes. *Anal. Biochem.* **144**: 593–603.
- Dizdaroglu M, Jaruga P, Birincioglu M, Rodriguez H. 2002. Free radical-induced damage to DNA: mechanisms and measurement. *Free Rad. Bio. Med.* **32**: 1102–1115.
- Drake PL, Hazelwood KJ. 2005. Exposure-related health effects of silver and silver compounds: a review. *Ann. Occup. Hyg.* **49**: 575–585.
- Dziendzikowska K, Gromadzka-Ostrowska J, Lankoff A, Oczkowski M, Krawczynska A, Chwastowska J, Sadowska-Bratek M, Chajduk E, Wojewodzka M, Dusinska M, Kruszewski M. 2012. Time-dependent biodistribution and excretion of silver nanoparticles in male Wistar rats. *J. Appl. Toxicol.* 2012; **32**: 920–928.
- Ellegaard-Jensen L, Jensen KA, Johansen A. 2012. Nano-silver induces dose-response effects on the nematode *Caenorhabditis elegans*. *Ecotoxicol. Environ. Saf.* **80**: 216–223.
- Evans MD, Dizdaroglu M, Cooke MS. 2004. Oxidative DNA damage and disease: induction, repair and significance. *Mutat. Res.* **567**: 1–61.
- Fabrega J, Fawcett SR, Renshaw JC, Lead JR. 2009. Silver nanoparticle impact on bacterial growth: effect of pH, concentration, and organic matter. *Environ. Sci. Technol.* **43**: 7285–7290.
- Fabrega J, Luoma SN, Tyler CR, Galloway TS, Lead JR. 2011. Silver nanoparticles: behaviour and effects in the aquatic environment. *Environ. Int.* **37**: 517–531.
- Ferguson M, Boyer M, Sprando R. 2010. A method for ranking compounds based on their relative toxicity using neural networking, *C. elegans*, axenic liquid culture, and the COPAS parameters TOF and EXT. *Open Access Bioinformatics* **2010**: 139–144.
- Foldbjerg R, Dang DA, Autrup H. 2011. Cytotoxicity and genotoxicity of silver nanoparticles in the human lung cancer cell line, A549. *Arch. Toxicol.* **85**: 743–750.
- Fung MC, Bowen DL. 1996. Silver products for medical indications: risk-benefit assessment. *J. Toxicol. Clin. Toxicol.* **34**: 119–126.
- Garigan D, Hsu AL, Fraser AG, Kamath RS, Ahringer J, Kenyon C. 2002. Genetic analysis of tissue aging in *Caenorhabditis elegans*: a role for heat-shock factor and bacterial proliferation. *Genetics* **161**: 1101–1112.
- Hadrup N, Loeschner K, Bergstrom A, Wilcks A, Gao X, Vogel U, Frandsen HL, Larsen EH, Lam HR, Mortensen A. 2012. Subacute oral toxicity investigation of nanoparticulate and ionic silver in rats. *Arch. Toxicol.* **86**: 543–551.
- HHS/NIH, HIEHS/NTP, NHGRI/NCGC, EPA/ORDFDA. 2010. Memorandum of Understanding on High Throughput Screening, Toxicity Pathway Profiling, and Biological Interpretation of Findings.
- Hunt PR, Olejnik N, Sprando RL. 2012. Toxicity ranking of heavy metals with screening method using adult *Caenorhabditis elegans* and propidium iodide replicates toxicity ranking in rat. *Food Chem. Toxicol.* **50**: 3280–3290.
- Hussain SM, Hess KL, Gearhart JM, Geiss KT, Schlager JJ. 2005. In vitro toxicity of nanoparticles in BRL 3A rat liver cells. *Toxicol. In Vitro* **19**: 975–983.
- Jaruga P, Rozalski R, Jawien A, Migdalski A, Olinski R, Dizdaroglu M. 2012. DNA damage products (5'R)- and (5'S)-8,5'-cyclo-2'-deoxyadenosines as potential biomarkers in human urine for atherosclerosis. *Biochemistry* **51**: 1822–1824.
- Kaletta T, Hengartner MO. 2006. Finding function in novel targets: *C. elegans* as a model organism. *Nat. Rev. Drug Discov.* **5**: 387–398.
- Karlsson HL. 2010. The comet assay in nanotoxicology research. *Anal. Bioanal. Chem.* **398**: 651–666.
- Rajapakse K, Drobne D, Kastelec D, Marinsek-Logar R. 2012. Experimental evidence of false-positive Comet test results due to TiO₂ particle - assay interactions. *Nanotoxicology*.
- Kawasaki M, Hisamoto N, Iino Y, Yamamoto M, Ninomiya-Tsuji J, Matsumoto K. 1999. A *Caenorhabditis elegans* JNK signal transduction pathway regulates coordinated movement via type-D GABAergic motor neurons. *EMBO J.* **18**: 3604–3615.
- Keene AM, Tyner KM. 2011. Analytical characterization of gold nanoparticle primary particles, aggregates, agglomerates, and agglomerated aggregates. *J. Nanopart. Res.* **13**: 3465–3481.
- Kim YS, Kim JS, Cho HS, Rha DS, Kim JM, Park JD, Choi BS, Lim R, Chang HK, Chung YH, Kwon IH, Jeong J, Han BS, Yu IJ. 2008. Twenty-eight-day oral toxicity, genotoxicity, and gender-related tissue distribution of silver nanoparticles in Sprague-Dawley rats. *Inhal. Toxicol.* **20**: 575–583.
- Kvitek L, Panacek A, Soukupova J, Kolar M, Vecerova R, Prucek R, Holecova M, Zboril R. 2008. Effect of Surfactants and Polymers on Stability and Antibacterial Activity of Silver Nanoparticles (NPs). *J. Phys. Chem. C* **112**: 5825–5834.
- Laboratory NER. 2010 *State of the Science Literature Review: Everything Nanosilver and More, Everything Nanosilver and More edn (EPA ESD ed.)*. U.S. Environmental Protection Agency; 1–145.
- Lee HY, Inselman AL, Kanungo J, Hansen DK. 2012. Alternative models in developmental toxicology. *Syst. Biol. Reprod. Med.* **58**: 10–22.
- Lin MH, Hsu TS, Yang PM, Tsai MY, Perng TP, Lin LY. 2009. Comparison of organic and inorganic germanium compounds in cellular radiosensitivity and preparation of germanium nanoparticles as a radiosensitizer. *Int. J. Radiat. Biol.* **85**: 214–226.
- Loeschner K, Hadrup N, Qvortrup K, Larsen A, Gao X, Vogel U, Mortensen A, Lam H, RLarsen EH. 2011. Distribution of silver in rats following 28 days of repeated oral exposure to silver nanoparticles or silver acetate. *Part. Fibre Toxicol.* **8**: 18.
- Lok CN, Ho CM, Chen R, He QY, Yu WY, Sun H, Tam PK, Chiu JF, Che CM. 2006. Proteomic analysis of the mode of antibacterial action of silver nanoparticles. *J. Proteome Res.* **5**: 916–924.
- Lok CN, Ho CM, Chen R, He QY, Yu WY, Sun H, Tam PK, Chiu JF, Che CM. 2007. Silver nanoparticles: partial oxidation and antibacterial activities. *J. Biol. Inorg. Chem.* **12**: 527–534.
- Matuk Y, Ghosh M, McCulloch C. 1981. Distribution of silver in the eyes and plasma proteins of the albino rat. *Can. J. Ophthalmol.* **16**: 145–150.
- Mei N, Zhang Y, Chen Y, Guo X, Ding W, Ali SF, Biris AS, Rice P, Moore MM, Chen T. 2012. Silver nanoparticle-induced mutations and oxidative stress in mouse lymphoma cells. *Environ. Mol. Mutagen.* **53**: 409–419.
- Meyer JN. 2010. QPCR: a tool for analysis of mitochondrial and nuclear DNA damage in ecotoxicology. *Ecotoxicology* **19**: 804–811.
- Meyer JN, Boyd WA, Azzam GA, Haugen AC, Freedman JH, Van Houten B. 2007. Decline of nucleotide excision repair capacity in aging *Caenorhabditis elegans*. *Genome Biol.* **8**: R70.
- Meyer JN, Lord CA, Yang XY, Turner EA, Badireddy AR, Marinakos SM, Chilkoti A, Wiesner M, RAuffan M. 2010. Intracellular uptake and associated toxicity of silver nanoparticles in *Caenorhabditis elegans*. *Aquat. Toxicol.* **100**: 140–150.

- Morones JR, Elechiguerra JL, Camacho A, Holt K, Kouri JB, Ramirez JT, Yacamán MJ. 2005. The bactericidal effect of silver nanoparticles. *Nanotechnology* **16**: 2346–2353.
- Nass R, Hamza I. 2007. The nematode *C. elegans* as an animal model to explore toxicology in vivo: solid and axenic growth culture conditions and compound exposure parameters. *Curr. Protoc. Toxicol.* **Chapter 1**: Unit1 9.
- Nel A, Xia T, Madler L, Li N. 2006. Toxic potential of materials at the nanolevel. *Science* **311**: 622–627.
- Oostingh GJ, Casals E, Italiani P, Colognato R, Stritzinger R, Ponti J, Pfaller T, Kohl Y, Ooms D, Favilli F, Leppens H, Lucchesi D, Rossi F, Nelissen I, Thielecke H, Puntjes VF, Duschl A, Boraschi D. 2011. Problems and challenges in the development and validation of human cell-based assays to determine nanoparticle-induced immunomodulatory effects. *Part. Fibre Toxicol.* **8**: 8.
- Pal S, Tak YK, Song JM. 2007. Does the antibacterial activity of silver nanoparticles depend on the shape of the nanoparticle? A study of the Gram-negative bacterium *Escherichia coli*. *Appl. Environ. Microbiol.* **73**: 1712–1720.
- Parry JM, Parry E, Phrakonkham P, Corvi R. 2010. Analysis of published data for top concentration considerations in mammalian cell genotoxicity testing. *Mutagenesis* **25**: 531–538.
- Percival SL, Bowler PG, Dolman J. 2007. Antimicrobial activity of silver-containing dressings on wound microorganisms using an in vitro biofilm model. *Int. Wound J.* **4**: 186–191.
- Petersen EJ, Nelson BC. 2010. Mechanisms and measurements of nanomaterial-induced oxidative damage to DNA. *Anal. Bioanal. Chem.* **398**: 613–650.
- Rao AU, Carta LK, Lesuisse E, Hamza I. 2005. Lack of heme synthesis in a free-living eukaryote. *Proc. Natl. Acad. Sci. U.S.A.* **102**: 4270–4275.
- Rodriguez H, Jurado J, Laval J, Dizdaroglu M. 2000. Comparison of the levels of 8-hydroxyguanine in DNA as measured by gas chromatography mass spectrometry following hydrolysis of DNA by *Escherichia coli* Fpg protein or formic acid. *Nucleic Acids Res.* **28**: 1–8.
- Rungby J, Danscher G. 1984. Hypoactivity in silver exposed mice. *Acta Pharmacol. Toxicol. (Copenh.)* **55**: 398–401.
- Samberg ME, Lobo EG, Oldenburg SJ, Monteiro-Riviere NA. 2012. Silver nanoparticles do not influence stem cell differentiation but cause minimal toxicity. *Nanomedicine (Lond.)* **7**: 1197–1209.
- Sayes CM, Reed KL, Warheit DB. 2007. Assessing toxicity of fine and nanoparticles: comparing in vitro measurements to in vivo pulmonary toxicity profiles. *Toxicol. Sci.* **97**: 163–180.
- Sondi I, Salopek-Sondi B. 2004. Silver nanoparticles as antimicrobial agent: a case study on *E. coli* as a model for Gram-negative bacteria. *J. Colloid Interface Sci.* **275**: 177–182.
- Sotiriou GA, Pratsinis SE. 2010. Antibacterial activity of nanosilver ions and particles. *Environ. Sci. Technol.* **44**: 5649–5654.
- Sprando RL, Olejnik N, Cinar HN, Ferguson M. 2009. A method to rank order water soluble compounds according to their toxicity using *Caenorhabditis elegans*, a Complex Object Parametric Analyzer and Sorter, and axenic liquid media. *Food Chem. Toxicol.* **47**: 722–728.
- Tuna G, Ozkaya F, Dizdaroglu M, Kirkali G. 2011. Oxidatively Induced DNA Base Damage and DNA Repair Enzyme Expression Levels in Alzheimer's Disease. *Free Radic. Biol. Med.* **51**: S32–S33.
- Wijnhoven SWP, Peijnenburg WJGM, Herberts CA, Hagens WI, Oomen AG, Heugens EHW, Roszek B, Bisschops J, Gosens I, Meent DVD, Dekkers S, Jong WHD, Zijverden Mv, Sips AJAM, Geertsma RE. 2009. Nano-silver – a review of available data and knowledge gaps in human and environmental risk assessment. *Nanotoxicology* **3**: 109–138.
- Willets KA, Van Duyne RP. 2007. Localized surface plasmon resonance spectroscopy and sensing. *Annu. Rev. Phys. Chem.* **58**: 267–297.
- Williams PL, Dusenbery DB. 1988. Using the nematode *Caenorhabditis elegans* to predict mammalian acute lethality to metallic salts. *Toxicol. Ind. Health* **4**: 469–478.
- Zhang Q, Kusaka Y, Zhu X, Sato K, Mo Y, Kluz T, Donaldson K. 2003. Comparative toxicity of standard nickel and ultrafine nickel in lung after intratracheal instillation. *J. Occup. Health* **45**: 23–30.